THE JOURNAL OF PHYSICAL CHEMISTRY B
A JOURNAL OF THE AMERICAN CHEMICAL SOCIETY

pubs.acs.org/JPCB

Article

Salt-Induced Transitions in the Conformational Ensembles of Intrinsically Disordered Proteins

Hiranmay Maity,[‡] Lipika Baidya,[‡] and Govardhan Reddy*

Cite This: *J. Phys. Chem. B* 2022, 126, 5959−5971

Read Online

ACCESS | Metrics & More | Article Recommendations | Supporting Information

ABSTRACT: Salts modulate the behavior of intrinsically disordered proteins (IDPs) and influence the formation of membraneless organelles through liquid−liquid phase separation (LLPS). In low ionic strength solutions, IDP conformations are perturbed by the screening of electrostatic interactions, independent of the salt identity. In this regime, insight into the IDP behavior can be obtained using the theory for salt-induced transitions in charged polymers. However, salt-specific interactions with the charged and uncharged residues, known as the Hofmeister effect, influence IDP behavior in high ionic strength solutions. There is a lack of reliable theoretical models in high salt concentration regimes to predict the salt effect on IDPs. We propose a simulation methodology using a coarse-grained IDP model and experimentally measured water to salt solution transfer free energies of various chemical groups that allowed us to study the salt-specific transitions induced in the IDPs conformational ensemble. We probed the effect of three different monovalent salts on five IDPs belonging to various polymer classes based on charged residue content. We demonstrate that all of the IDPs of different polymer classes behave as self-avoiding walks (SAWs) at physiological salt concentration. In high salt concentrations, the transitions observed in the IDP conformational ensembles are dependent on the salt used and the IDP sequence and composition. Changing the anion with the cation fixed can result in the IDP transition from a SAW-like behavior to a collapsed globule. An important implication of these results is that a suitable salt can be identified to induce condensation of an IDP through LLPS.

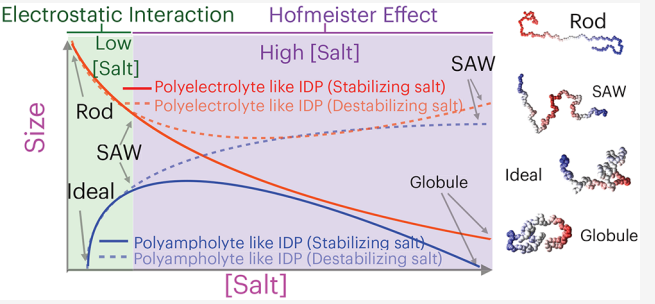

INTRODUCTION

Salts have significant impact on the conformations sampled by intrinsically disordered proteins/regions (IDPs/IDRs). As a result, salts can affect diverse cellular functions of IDPs[1] such as cell signaling,[2] stress granule assembly,[3,4] heterochromatin formation,[5] transcription, etc. Furthermore, transitions in the conformational ensembles sampled by IDPs due to the changes in cellular environment can result in pathologies[4,6] such as neurodegenerative diseases and cancer[7] through the formation of membraneless organelles[8] via liquid−liquid phase separation (LLPS).[9]

Salts modulate a range of biophysical processes such as protein folding, aggregation, protein−RNA interactions, protein crystallization, and precipitation.[10,11] The mechanism through which salts interact with biomolecules depends on the salt concentration ([salt]). In low [salt], the ions screen the electrostatic interactions between the charged residues independent of the salt used. However, in high [salt], the ions interact with the biomolecules through salt-specific interactions known as Hofmeister effects. Salt ions are arranged in a series referred to as Hofmeister series based on their ability to stabilize/destabilize (salting-out/-in) the folded state of a globular protein.[11−14]

At physiological conditions, IDPs rapidly interconvert between nonspecific conformations as they are devoid of secondary/tertiary structures due to a significant fraction of polar and charged residues present in their sequences.[15] There has been extensive effort using experiments and theory to understand the effect of salts on the IDPs.[16−19] Single-molecule Förster energy transfer (smFRET) and simulations demonstrated that, in low ionic strength solutions, the dimensions of the IDPs increased with the net charge.[16,17,20] Polyampholyte-like IDPs exhibited compaction in dimensions due to interaction between opposite charges.[20−24] Experiments further demonstrated using the polymer scaling laws that solvent quality of water to the IDPs depends on the IDP sequence composition.[18,25] However, it is challenging to characterize the conformational ensembles sampled by IDPs as they are highly influenced by the charge distribution in the sequence. The charge distribution in the IDPs can be characterized by parameters such as the fraction of charged residues (FCR), the net charge per residue (NCPR), charge

Received: May 19, 2022
Revised: July 22, 2022
Published: August 9, 2022

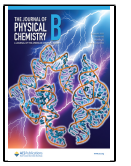

https://doi.org/10.1021/acs.jpcb.2c03476
J. Phys. Chem. B 2022, 126, 5959−5971

asymmetry ($\sigma_{\pm}$), charge pattern (κ), and sequence charge decoration (SCD)[21,23,24,26,27] (see Methods for details). These parameters further help identify the IDPs to the polymer class they belong to, such as polyelectrolytes, polyampholytes, or uncharged polymers.

Since charge distribution in the IDPs plays a critical role in influencing their conformational ensemble, salts will significantly impact IDP conformations and their physical properties. In low [salt] solutions, salts affect the IDP conformations through charge screening, independent of the salt identity. Therefore, we can exploit the existing polyelectrolyte[28−31] and polyampholyte[22,26,32,33] theories to understand the IDP behavior as demonstrated previously.[16,22,27] However, in large [salt], salt identity is crucial due to the salt-specific Hofmeister effects[11,34] that affect the IDP conformations. There is no analytic theory to account for the Hofmeister effects on IDPs. A recent coarse-grained hydrophobicity scale (HPS) model[19] parametrized using the FRET efficiency experimental data was able to predict the salt effect on the LLPS of IDPs.

Computer simulations complement experiments and theory and are playing an important role in elucidating the behavior of IDPs. Simulations were pivotal in understanding the IDPs conformational ensembles and dynamics.[20−22,35−44] Computer simulations using atomistic force fields matching the appropriate length and time scales of the biophysical phenomena have the advantage of providing detailed information about the biophysical processes.[45−49] However, the main drawbacks are the lack of reliable all-atom force fields[50] to simulate the Hofmeister effect of salts, and it is computationally intensive to simulate large IDPs to obtain conformations representative of the equilibrium ensembles.

In this article, we developed an efficient simulation model to compute the properties of IDPs in different salt concentration regimes and studied salt-induced transitions in the conformational ensembles of different classes of IDPs. To overcome the time scale problem associated with the sampling of representative IDP conformations, we used a coarse-grained model for the IDPs, which is a variant of the self-organized polymer model for IDP (SOP-IDP).[35] The effect of salt on the IDP residues is taken into account implicitly using the molecular transfer model.[51,52] The transfer energies of amino acids in various salt solutions are obtained from the experiments,[34,53] where the salt's effect on the solubility of model compounds used to mimic amino acids is measured and explained in terms of the solute partitioning model.[54] We have successfully used this model in a previous study to probe the effect of salts on protein folding thermodynamics.[55]

To understand salt-induced transitions in the conformational ensembles of IDPs, we studied the effect of salt on the conformations of five different IDPs: (1) nucleoporin, (2) human prothymosin-α, (3) cyclin-dependent inhibitor kinase sic1, (4) N-terminal transactivation domain (TADn) of ERM protein (ERMTADn), and (5) N-terminal domain of HIV-1 integrase (IN). These IDPs have different chain lengths (N_{res}), compositions, sequences, and physicochemical properties based on the electrolytic behavior (Supporting Information Table S1). These IDPs are also used as model systems in experiments[16,56−59] to understand IDP properties. Nucleoporin is an 81 residue long uncharged IDP rich in hydrophilic residues. The other IDP sequences contain ionizable charged residues and behave as polyelectrolytes or polyampholytes, depending on their NCPR and FCR. Human prothymosin-α and sic1 are polyelectrolytes, whereas ERMTADn and IN are polyampholytes. In the absence of Zn^{2+}, IN is unstructured, and in this study, we treat it like an IDP. The IDP sequences are characterized[21,60] using FCR, NCPR, and $\sigma_{\pm}$ (Table S1). To probe the effect of salts on IDPs, we performed simulations of IDPs in three different salt solutions: guanidine hydrochloride (GuHCl), potassium chloride (KCl), and potassium glutamate (KGlu). The salt GuHCl acts as a denaturant, which destabilizes a globular protein's folded state, whereas KCl and KGlu are protective osmolytes, which stabilize the folded state. Experiments[16,18] on IDPs show that GuHCl stabilizes the expanded conformations, whereas KCl and KGlu stabilize the compact conformations.

METHODS

We used a variant of the self-organized polymer model for intrinsically disordered proteins (SOP-IDP) to model the IDPs.[35] The SOP-IDP model is similar to the well-established self-organized polymer model with side chains (SOP-SC),[52,61] which is extensively used to study folding thermodynamics of globular proteins.[62−67] In SOP-IDP, each residue is modeled as two beads—one bead for the backbone atoms and the other bead for side chain atoms. The center of backbone bead is present at the C_α position, and the center of the side chain bead is present at the center of mass of the side chain atoms. The primary sequence of the five IDPs used in this study is shown in Table S1. Initial structures for the two bead SOP-IDP model are generated using VMD.[68]

The energy function ($E_{CG}(\{\mathbf{r}\}, 0)$) of the SOP-IDP model in the absence of salt-specific Hofmeister effects is the sum of bonded (E_B), nonbonded (E_{NB}), and electrostatic (E_{ele}) interactions. The nonbonded energy consists of local (E_{NB}^{L}) and nonlocal (E_{NB}^{NL}) interactions. The Hamiltonian of the SOP-IDP model is

$$E_{CG}(\{\mathrm{r}\}, 0) = E_B + E_{NB}^{L} + E_{NB}^{NL} + \lambda E_{ele} \tag{1}$$

If charged residues are present in the IDP, then $\lambda = 1$; else, $\lambda = 0$. The bonded potential E_B between two beads, which are connected by a covalent bond, is modeled using the finite extensible nonlinear elastic (FENE) potential,

$$E_B = -\sum_{i=1}^{N_B} \frac{k}{2} {R_0}^2 \log\left(1 - \frac{(r_i - r_i^0)^2}{{R_0}^2}\right) \tag{2}$$

where N_B is the total number of bonds in the SOP-IDP model. r_i is the instantaneous bond distance between the ith pair of bonded beads, r_i^0 is their corresponding equilibrium bond distance, and R_0 is the maximum tolerance of bond extension/compression. The values of r_i^0 are set to the initial bond distance values obtained from VMD. The values of k and R_0 are given in Table S2. The two beads, which are not bonded by a covalent bond and separated by less than two residues along the polypeptide chain, interact with each other through a nonbonded local potential (E_{NB}^{L}). E_{NB}^{L} is a purely repulsive potential accounting for excluded volume interactions to prevent unphysical overlap between the two nonbonded beads and is given by

$$E_{NB}^{L} = \sum_{i=1}^{N_l} \epsilon_l \left(\frac{\sigma_i}{r_i}\right)^6 \tag{3}$$

where σ_i is the sum of the van der Waals (vdW) radii of the ith pair of nonbonded beads and ϵ_l is the strength of repulsive

https://doi.org/10.1021/acs.jpcb.2c03476
J. Phys. Chem. B 2022, 126, 5959−5971

interaction. The value of ϵ_l is given in Table S2, and values of vdW radii for each amino acid residue are listed in Table S3.

The beads, which are separated by more than two residues, interact through nonbonded nonlocal interaction potential, E_{NB}^{NL}, which is modeled using

$$E_{NB}^{NL} = \sum_{i=1}^{N_{bb}} \omega \times 300k_B \times |0.7 - \epsilon_i^{bb}| \left[\left(\frac{\sigma^{bb}}{r_i}\right)^{12} - 2\left(\frac{\sigma^{bb}}{r_i}\right)^{6}\right] + \sum_{i=1}^{N_{bs}} \omega \times 300k_B \times |0.7 - \epsilon_i^{bs}| \left[\left(\frac{\sigma_i^{bs}}{r_i}\right)^{12} - 2\left(\frac{\sigma_i^{bs}}{r_i}\right)^{6}\right] + \sum_{i=1}^{N_{ss}} \omega \times 300k_B \times |0.7 - \epsilon_i^{ss}| \left[\left(\frac{\sigma_i^{ss}}{r_i}\right)^{12} - 2\left(\frac{\sigma_i^{ss}}{r_i}\right)^{6}\right] \quad (4)$$

The first, second, and third terms of eq 4 correspond to the backbone−backbone, backbone−side chain, and side chain−side chain interactions energies, respectively. N_{bb}, N_{bs}, and N_{ss} denote the number of interaction pairs present between backbone−backbone, backbone−side chain, and side chain−side chain beads, respectively. r_i is the distance between the ith pair of beads, and k_B is the Boltzmann constant. σ^{bb} is the diameter of the backbone bead, which is taken as 3.8 Å. σ_i^{bs} and σ_i^{ss} are the sums of bead radii for the ith pair of backbone−side chain and side chain−side chain beads, respectively. σ_i^{bs} and σ_i^{ss} are computed using the bead radii listed in Table S3. ϵ_i^{bb}, ϵ_i^{bs}, and ϵ_i^{ss} are the strengths of backbone−backbone, backbone−side chain, and side chain−side chain interactions, respectively. We used Betancourt−Thirumalai statistical potential for ϵ_i^{ss}, which was initially proposed for the side chain−side chain interactions of globular proteins.[69] However, for IDPs we used a rescaling factor ω ($0 < \omega < 1$) to weaken the strength of interactions. The value of ϵ_i^{bb} is approximated to be the Betancourt−Thirumalai statistical potential corresponding to the interaction between two Gly residues. ϵ_i^{bs} is approximated as the statistical potential for the interaction between Gly and the side chain corresponding to the other residue. We have used an ω value for which the experimental and simulated SAXS profiles of the IDPs are in agreement. The value of ω used for all of the IDPs is given in Table S2. We have used the truncated and shifted form of Lennard-Jones (LJ) potential using a cutoff distance 30 Å beyond which the interaction between the two beads is neglected.

If an IDP contains charged residues, the beads corresponding to the side chains of the charged residues interact through a screened Coulomb potential given by

$$E_{ele} = \sum_{i=1}^{N_c-1} \sum_{j>i}^{N_c} \frac{q_i q_j \exp(-\kappa r_{ij})}{\epsilon r_{ij}} \quad (5)$$

where N_c is the total number of charged residues present in the IDP, r_{ij} is the distance between charged beads i and j, and q_i and q_j are the point charges measured in units of electron charge placed on the centers of the side chain beads i and j, respectively. At neutral pH, q_i is +1 for positively charged Lys and Arg residues and −1 for negatively charged Asp and Glu residues. The inverse Debye length, κ, is computed for 150 mM monovalent salt concentration. We have used the dielectric constant of the medium $\epsilon = 78.0\ \epsilon_0$, where ϵ_0 (=1.0) is the permittivity of vacuum.

The energy functions and the parameters accounting for the interaction strength used in this article are the same as the SOP-IDP model[35,70] except for the nonlocal nonbonded potential (E_{NB}^{NL}). The energy functions used to describe E_{NB}^{NL} (eq 4) are the same in both models, but the parameters which account for the interaction strength between a pair of nonlocal beads are different. We also introduced residue-specific backbone−side chain interactions in addition to the residue-specific side chain−side chain interactions.

Molecular Transfer Model (MTM). Salts in low concentration affect the IDP conformations by screening the electrostatic interactions, and this effect is independent of the salt identity but depends on the salt concentration ([salt]), whereas, in high concentration, salts affect the IDP conformations through salt-specific Hofmeister effects. The nonspecific Coulombic interaction is modeled by the E_{ele} potential (eq 5).

To introduce salt-specific interactions, we used the molecular transfer model (MTM), which was extensively used previously to study folding thermodynamics of globular proteins.[55] In MTM, the modified energy function of an IDP conformation with coordinates ($\{\mathbf{r}\}$) and salt concentration [salt] is given by

$$E_{CG}(\{\mathbf{r}\}, [\text{salt}]) = E_{CG}(\{\mathbf{r}\}, 0) + \Delta G_{tr}(\{\mathbf{r}\}, [\text{salt}]) \quad (6)$$

where $\Delta G_{tr}(\{\mathbf{r}\},[\text{salt}])$ is the transfer free energy associated with the transferring of an IDP conformation from water to a salt solution with concentration [salt] and is given by

$$\Delta G_{tr}(\{\mathbf{r}\}, [\text{salt}]) = \sum_{i=1}^{N_{res}} \delta g_{tr}^{bb}([\text{salt}]) \frac{\alpha_i^{bb}(\{\mathbf{r}\})}{\alpha_{Gly-i-Gly}^{bb}} + \sum_{i=1}^{N_{res}} \delta g_{tr,i}^{sc}([\text{salt}]) \frac{\alpha_i^{sc}(\{\mathbf{r}\})}{\alpha_{Gly-i-Gly}^{sc}} \quad (7)$$

where N_{res} is the total number of residues in the IDP, $\delta g_{tr}^{bb}([\text{salt}])$ and $\delta g_{tr,i}^{sc}([\text{salt}])$ are the transfer free energies of backbone bead and side chain bead of the ith residue from water to a salt solution [salt], respectively, $\alpha_i^{bb}(\{\mathbf{r}\})$ and $\alpha_i^{sc}(\{\mathbf{r}\})$ are the solvent accessible surface areas (SASAs) of the backbone and side chain beads of residue i in the protein chain, and $\alpha_{Gly-i-Gly}^{bb}$ and $\alpha_{Gly-i-Gly}^{sc}$ are the SASAs of the backbone and side chain beads of the same amino acid residue i in the tripeptide Gly−i−Gly. The values of $\delta g_{tr}^{bb}([\text{salt}])$, $\delta g_{tr,i}^{sc}([\text{salt}])$, $\alpha_{Gly-i-Gly}^{bb}$, and $\alpha_{Gly-i-Gly}^{sc}$ are available in ref 55. The SASA of IDP conformations is calculated using the method described by Wodak and Janin.[71]

In this model, electrostatic interactions are modeled using screened Coulomb potential, and the salt-specific effect on the IDP residues is taken into account using MTM.[51,52,55] The transfer energies of amino acids in different salts are available in ref 55.

Detailed descriptions of the SOP-IDP energy parameters are given in the Supporting Information.

Data Analysis. We ran low friction Langevin dynamics simulations of the IDPs using the SOP-IDP model in different salt concentrations. The IDP ensemble in the presence of salt is characterized using the small-angle X-ray scattering (SAXS) intensity profiles ($I(q)$), and it is calculated using the equation

$$I(q) = \sum_{i=1}^{N} \sum_{j=1}^{N} f_i(q) f_j(q) \frac{\sin(qr_{ij})}{qr_{ij}} \quad (8)$$

where q is the wave vector and its range is usually between 0 and 10 nm^{-1} in the experiments, r_{ij} is the distance between the

https://doi.org/10.1021/acs.jpcb.2c03476
J. Phys. Chem. B 2022, 126, 5959−5971

beads i and j, N is the number of beads in the IDP, and $f_i(q)$ is the form factor of bead i, and their values are taken from ref 72. The normalized structure factor,[73] $S(q)$, is computed using the equation

$$S(q) = \frac{1}{N_{bb}^{\ 2}} \sum_{i=1}^{N_{bb}} \sum_{j=1}^{N_{bb}} \frac{\sin(qr_{ij})}{qr_{ij}} \tag{9}$$

where N_{bb} is the number of backbone beads in the IDP and r_{ij} is the distance between the backbone beads of residues i and j. To characterize the changes in IDP dimensions with the change in salt concentration, we computed the radius of gyration of the IDP conformations using the equation

$$R_g = \left(\frac{1}{2N^2} \sum_{i,j} \vec{r}_{ij}^{\ 2} \right)^{1/2} \tag{10}$$

where $\vec{r}_{ij}$ is the vector joining beads i and j.

IDP Characterization. The IDP dimensions are characterized by the fraction of charged residues, FCR = $(f_+ + f_-)$ and net charge per residue, NCPR = $|f_+ - f_-|$, where f_+ and f_- are the fractions of positive and negative charged residues in the IDP. The charge asymmetry in the IDP is defined as $\left(\sigma_\pm = \frac{(f_+ - f_-)^2}{(f_+ + f_-)}\right)$. IDPs can be classified as polyelectrolytes (FCR > 0; NCPR > 0), polyampholytes (FCR > 0; NCPR ~ 0), and uncharged (FCR = NCPR = 0). Polyelectrolye- and polyampholyte-like IDPs are further categorized as weak (FCR ≤ 0.3) and strong (FCR > 0.3).[21,60]

In polyampholytes, segregation of positively and negatively charged residues are quantified in terms of charge patterning parameter (κ)[21] and sequence charge decoration[23,24] (SCD). κ is a measure of the deviation of local charge asymmetry of the blob (charged sequence segment) from the total charge asymmetry of the whole sequence. The range of κ is between 0 (well-mixed sequence) and 1 (segregated sequence). SCD also quantifies charge patterning, and it is defined as

$$\mathrm{SCD} = \frac{1}{N} \sum_{m=2}^{N} \sum_{n=1}^{m-1} q_m q_n (m-n)^{1/2} \tag{11}$$

where N is the number of charged residues and q_m and q_n are the charges of the mth and nth charged residues. SCD becomes more negative with increasing segregation of charged residues. $\mathrm{SCD}_{\mathrm{low\,salt}}$ characterizes IDP behavior as a function of [salt] in the low [salt] regime by quantifying charge patterning, and it is defined as

$$\mathrm{SCD}_{\mathrm{low\,salt}} = \frac{1}{N} \sum_{m=2}^{N} \sum_{n=1}^{m-1} q_m q_n (m-n) \tag{12}$$

where N is the number of charged residues and q_m and q_n are the charges on the mth and nth charged residues. IDPs with negative (positive) $\mathrm{SCD}_{\mathrm{low\,salt}}$ expand (compact) with increasing [salt] in the low [salt] regime.

RESULTS AND DISCUSSION

Kratky Plot of IDPs. We computed a normalized intensity of scattered wave vector ($I(q)/I(0)$) (eq 8) and a Kratky plot ($q^2 I(q)/I(0)$) for all five IDPs using the simulation data at T = 300 K and [salt] = 0.15 M. The computed $I(q)/I(0)$ and $q^2 I(q)/I(0)$ are in near quantitative agreement with the measurements from small-angle X-ray scattering[56−59] (SAXS) experiments in similar salt concentrations (Figures 1A,B and S1). The agreement between simulations and experiments for both smaller ($q \lesssim 1.0$ nm^{-1}) and larger q values ($q \gtrsim 1.0$ nm^{-1}) shows that the SOP-IDP model can capture the IDP's overall dimensions and accurately describe its structure at smaller length scales. The computed average radius of gyration ($\langle R_g^{sim} \rangle$) and the experimentally measured values (R_g^{exp}) of IDPs are in good agreement (Figure 1C). The Kratky plot of globular proteins exhibits a bell shaped curve due to the secondary and tertiary structures present in the protein. The Kratky plot of the IDPs exhibit a plateau at intermediate q values and further increases at larger q values, indicating the absence of ordered structure (Figure 1A,B).

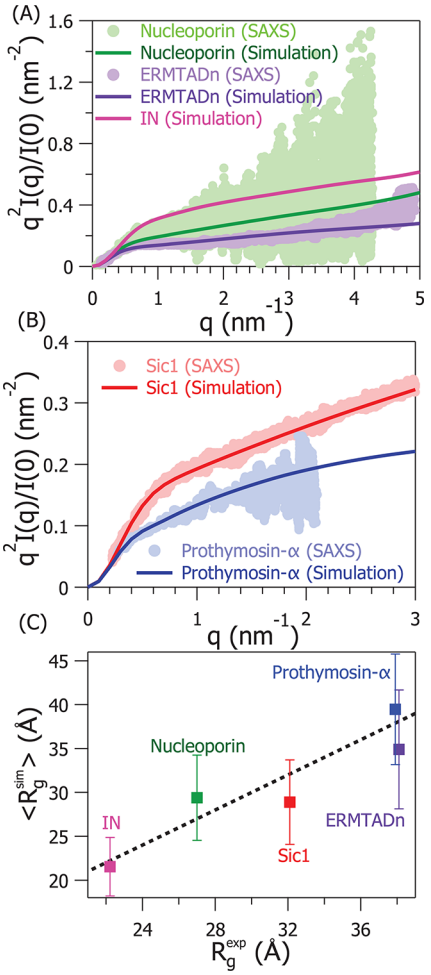

Figure 1. Normalized Kratky plot ($q^2 I(q)/I(0)$ vs q) from experiments and simulations for (A) nucleoporin (green), ERMTADn (violet), and IN (magenta) and (B) sic1 (red) and prothymosin-α (blue). Experimental data are not available for IN. Light shaded dots and deep solid line are the corresponding experimental and simulated results, respectively. (C) IDPs average radius of gyration computed from simulation, $\langle R_g^{sim} \rangle$, are plotted against the experimentally measured values, R_g^{exp}. The Pearson correlation coefficient is ≈0.93.

IDPs Exhibit Self-Avoiding Walk (SAW) Behavior and Conformational Heterogeneity at Physiological Salt Concentration. The scaling exponent ν, which indicates the polymer behavior in a solvent, is extracted using the scaling relation $R_{|i-j|} \sim |i-j|^{\nu}$, where $R_{|i-j|}$ is the distance between residues i and j in the IDP. The exponent ν is also extracted from the IDP backbone structure factor (eq 9) using the

https://doi.org/10.1021/acs.jpcb.2c03476
J. Phys. Chem. B 2022, 126, 5959−5971

scaling relation $S(q) \sim q^{-1/\nu}$.[73] The value of ν obtained from both methods is ≈0.59, suggesting that IDPs behave like a polymer in a good solvent exhibiting the features of a SAW at physiological salt concentration (≈150 mM) (Figure 2A,B).[22] The scaling exponent ν is strictly valid to describe the homopolymer behavior in different solvent conditions and holds only for polymers with a degree of polymerization, $N \gg 1$. Computing the exponent ν for the IDPs is an approximation, and it is only an effective way to characterize the IDP behavior in various solvent conditions. IDPs are heteropolymers, and their conformational ensembles are highly heterogeneous in nature,[35,37,74−77] which cannot be completely captured by the scaling exponents alone. We demonstrated the conformational heterogeneity in the IDPs by comparing their probability distribution of dimensionless end-to-end distance $X\left(=\frac{R_{ee}}{\sqrt{\langle R_{ee}^2\rangle}}\right)$, where R_{ee} is the end-to-end distance and $\langle R_{ee}^2\rangle$ is the second moment of the end-to-end distance) with the theoretically obtained universal expression for SAW[78] (Figure 2C). The universal shape of $P(X)$ for the SAW is given by

$$P(X) = 4\pi A X^{2+g} \exp[-\alpha X^{\delta}] \quad (13)$$

where ν is the Flory scaling exponent, $g = (\gamma - 1)/\nu$, $\delta = 1/(1 - \nu)$, and $\gamma \approx 1.1619$ for three-dimensional SAW.[79] The constants A and α are obtained using the constraints $\int_0^\infty P(X)\,dX = \int_0^\infty X^2 P(X)\,dX = 1$. The simulated $P(X)$ deviates significantly from the universal distribution, which can be attributed to the residue-specific interactions and long-range electrostatic interactions between the charged residues. In addition to $P(X)$, the nonlocal contact (contact between two residues separated by ≥8 residues along the polypeptide chain) frequency obtained for a pair of residues is inhomogeneous unlike a homopolymer, which further indicates that IDPs sample a heterogeneous ensemble (Figure S2). The IDPs heteropolymeric behavior can also be quantified by computing the deviation in the residue-specific distance[33] between two residues i and j with respect to an ideal polymer chain (Figure S3). The deviation is defined as

$$x_{ij} = \frac{\langle R_{ij}^2\rangle}{|i - j|l^2} \quad (14)$$

where R_{ij} is the distance between two specific residues i and j, l is the bond length between two backbone beads, and $|i - j|l^2$ is the distance between the identical residues in an ideal polymer chain. x_{ij} computed for different residue pairs in the IDPs is non-uniform and strongly depends on the sequence, suggesting heteropolymeric behavior of the IDPs (Figure S3).

Electrostatic Interactions and Hofmeister Effects Modulate IDP Behavior in Low and High Salt Concentration Regimes. To probe salt-induced transitions in the conformational ensembles of IDPs, we simulated IDPs in salt solutions of GuHCl, KCl, and KGlu. The salt GuHCl acts as a denaturant and destabilizes the folded state of globular proteins, whereas KCl and KGlu act as protective osmolytes, which stabilize the folded state.[16,18]

Salts modulate the IDPs behavior through the screening of electrostatic interactions and Hofmeister effects.[11,34] In low salt concentrations ([salt] < 1.0 M), the effect of salt on the IDP is primarily through the screening of electrostatic interactions, and it is independent of the identity of the salt. However, in high salt concentrations ([salt] ≥ 1.0 M), the effect of salt on the IDP is through Hofmeister effects, and it is salt-specific.[11,34] To demonstrate this in the simulations, we performed different sets of simulations using the energy

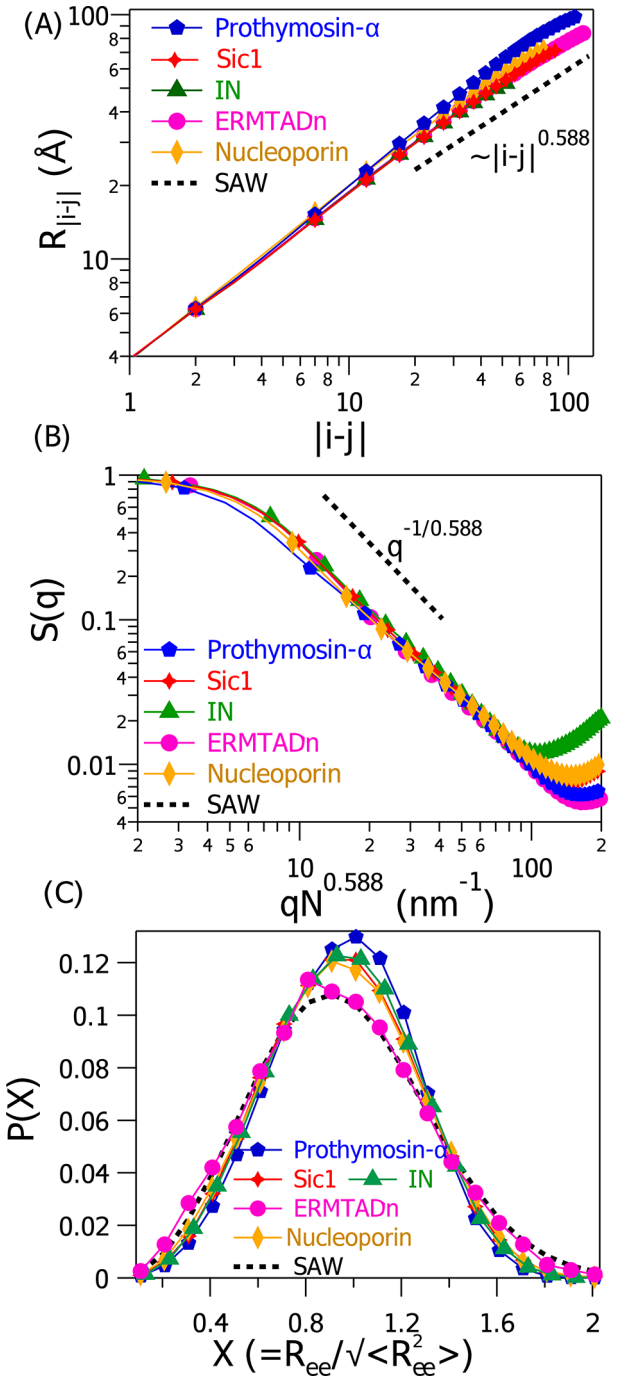

Figure 2. (A) Inter-residue distance ($R_{|i-j|}$) plotted as a function of separation between residues i and j ($|i - j|$) on a log−log scale for prothymosin-α (blue pentagons), sic1 (red diamonds), IN (green triangles), ERMTADn (magenta circles), and nucleoporin (yellow rhombus). The dotted line in black corresponds to a polymer exhibiting SAW for which $R_{|i-j|} \sim |i - j|^{0.588}$. (B) Structure factor ($S(q)$) for all five IDPs plotted as a function of scaled wave vector ($qN^{0.588}$), where N is the number of residues in the IDP. The dotted line in black corresponds to a polymer behaving as a SAW for which $S(q) \sim q^{-1/0.588}$. (C) Probability distribution of X $(=R_{ee}/\sqrt{\langle R_{ee}^2\rangle})$, $P(X)$, plotted for all five IDPs. The universal $P(X)$ for SAW (eq 13) is shown in black dashed line.

https://doi.org/10.1021/acs.jpcb.2c03476
J. Phys. Chem. B 2022, 126, 5959−5971

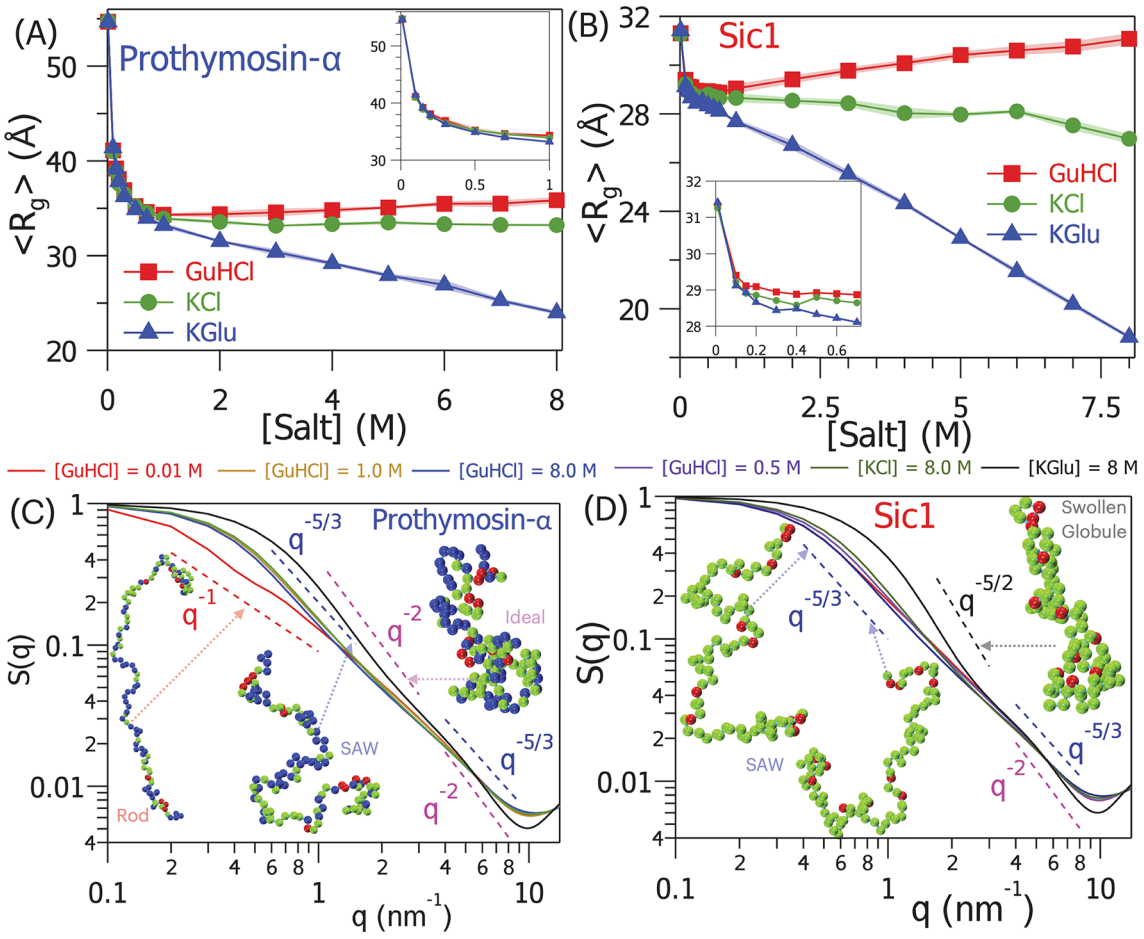

Figure 3. Average radius of gyration ($\langle R_g \rangle$) of (A) prothymosin-α and (B) sic1 computed as a function of [GuHCl] (red squares), [KCl] (green circles), and [KGlu] (blue triangles). $\langle R_g \rangle$ as a function of [salt] in low [salt] regime ($0 < [\text{salt}] \leq 1$ M) is shown in the inset. (C) Normalized structure factor $S(q)$ of prothymosin-α at [GuHCl] = 0.01 M (red), 1.0 M (yellow), and 8 M (blue); [KCl] = 8 M (green); and [KGlu] = 8.0 M (black). (D) $S(q)$ for sic1 at [GuHCl] = 0.01 M (red), 0.5 M (violet), and 8 M (blue); [KCl] = 8 M (green); and [KGlu] = 8.0 M (black). The dashed straight lines with scaling q^{-1}, $q^{-5/3}$, $q^{-5/2}$, and q^{-2} correspond to rod-like (red), SAW (blue), swollen globule (black), and, ideal (magenta) configurations. Representative IDP structure(s) are shown in bead representation. The acidic, basic, and neutral residues are shown as blue, red, and green beads, respectively.

functions, eq 1 and 6. When we simulate the IDP using the energy function given by eq 1, we take into account only the screening of the electrostatic interactions in the IDP due to the addition of the salt. However, when we simulate the IDP using the energy function given by eq 6, we include the transfer energy ($\Delta G_{tr}(\{\mathbf{r}\},[\text{salt}])$) in the energy function, which takes into account the salt-specific Hofmeister effects on the IDP. Simulations show that the average radius of gyration ($\langle R_g^{ele} \rangle$) (eq 10) for a charged IDP initially increases or decreases due to charge screening for [salt] < 1 M when simulations are performed using eq 1 (Figure S4). For [salt] ≥ 1 M, the effect of charge screening on $\langle R_g^{ele} \rangle$ is minimal. However, on adding the $\Delta G_{tr}(\{\mathbf{r}\},[\text{salt}])$ term to the energy function (eq 6), the average radius of gyration ($\langle R_g \rangle$) of the IDPs increased in the case of GuHCl, which acts as a denaturant for folded proteins for [GuHCl] > 1 M due to salt-specific Hofmeister effect (Figure S4). This demonstrates that initially the effect of salt on the IDP is due to the salt identity independent screening of electrostatic interactions, and in high [salt] the effect on the IDP is due to the salt-specific Hofmeister effect[34] (Figures 3, 4, and 5).

Salt-Induced Transitions in Polyelectrolyte-like IDPs. We characterized the structures of polyelectrolyte-like IDPs, prothymosin-α and sic1, as a function of [salt]. In the low [salt] regime ([salt] < 1 M), the $\langle R_g \rangle$ of the IDPs initially decreased with an increase in [salt] due to charge screening (Figure 3A,B). The decrease in $\langle R_g \rangle$ with an increase in [salt] followed the same trend obtained for polyelectrolytes in monovalent [salt].[22,28,29,31,80] The decrease in $\langle R_g \rangle$ for prothymosin-α and sic1 with the increase in [salt] from 0 to 0.7 M is ≈20.1 and 2.5 Å, respectively, and this initial compaction due to charge screening is independent for the three salts (GuHCl, KCl, and KGlu) used. The effect of [salt] on the dimension of a charged IDP can be assessed using FCR or NCPR.[20] Prothymosin-α is a strong polyelectrolyte (FCR ≈ 0.57; NCPR ≈ 0.39), whereas sic1 is a weak polyelectrolyte (FCR ≈ 0.12; NCPR ≈ 0.12). The extent of compaction in the IDP dimensions observed for prothymosin-α and sic1 can be attributed to their strong and weak polyelectrolyte behavior.

In the high [salt] regime ([salt] > 1 M), the increase or decrease in the IDP dimensions depends on the Hofmeister effect of the salt. Salt GuHCl stabilizes expanded IDP conformations, and the dimensions of both prothymosin-α and sic1 increased with the increase in [GuHCl], whereas salts KCl and KGlu stabilized compact IDP conformations and the dimensions of both prothymosin-α and sic1 decreased with the

https://doi.org/10.1021/acs.jpcb.2c03476
J. Phys. Chem. B 2022, 126, 5959−5971

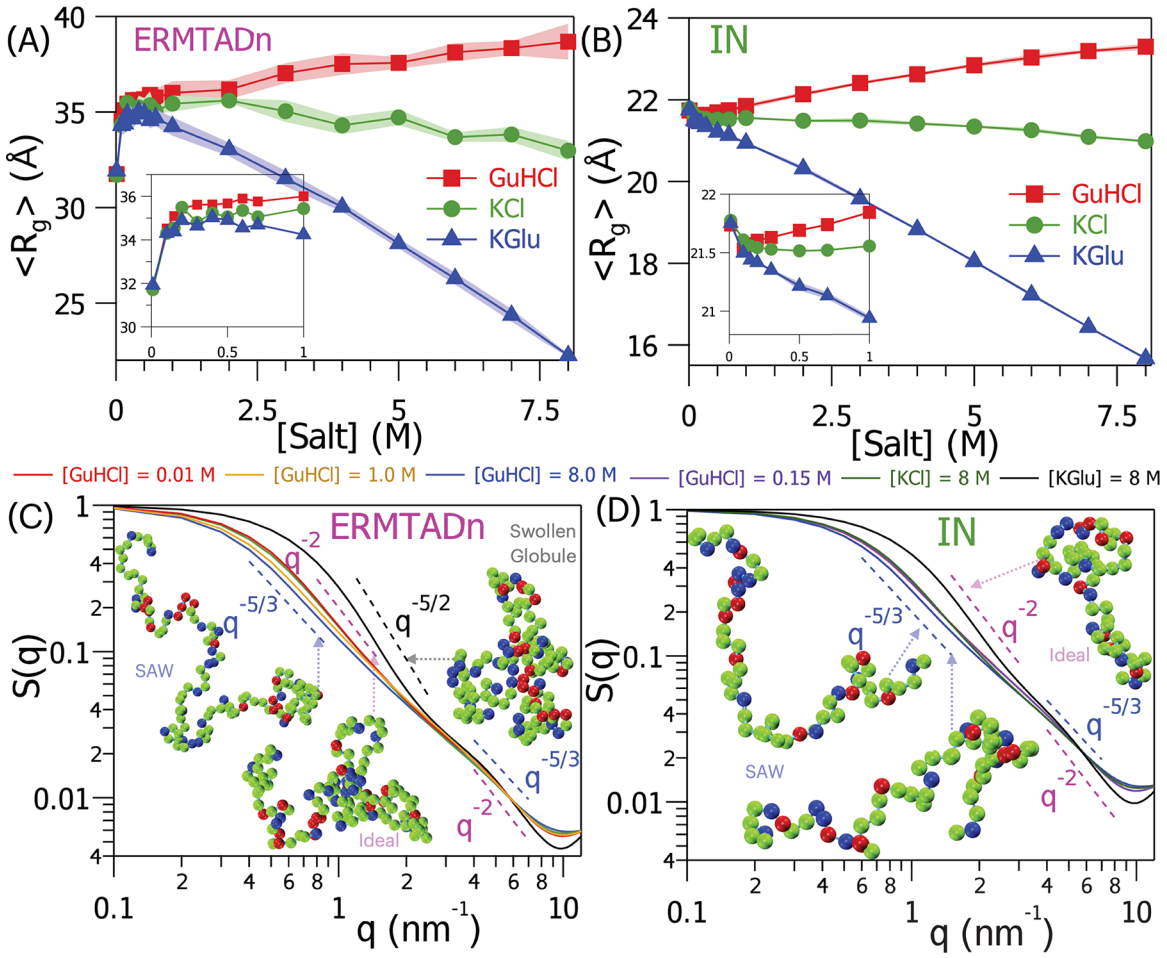

Figure 4. $\langle R_g \rangle$ of (A) ERMTADn and (B) IN computed in the presence of [GuHCl] (red squares), [KCl] (green circles), and [KGlu] (blue triangles). $\langle R_g \rangle$ as a function of [salt] in low [salt] regime is shown in the inset. (C) $S(q)$ of ERMTADn in the presence of [GuHCl] = 0.01 M (red), 1 M (yellow), and 8 M (blue); [KCl] = 8 M (green); and [KGlu] = 8 M (black). (D) $S(q)$ of IN computed in the presence of [GuHCl] = 0.01 M (red), 0.15 M (violet), and 8 M (blue); [KCl] = 8 M (green); and [KGlu] = 8 M (black). The dashed straight lines with $q^{-5/3}$, q^{-2}, and $q^{-5/2}$ represent SAW (blue), an ideal chain (magenta), and a swollen globule (black), respectively. Representative structure(s) of IDPs are shown in bead representation. The acidic, basic, and neutral residues are color coded as blue, red, and green beads, respectively.

increase in [KCl] or [KGlu]. KGlu strongly stabilizes compact conformations of the IDPs compared to KCl. The extent of prothymosin-α and sic1 compaction in the presence of KGlu is larger compared to KCl (Figure 3A,B). Experiments,[16] theory,[28,29,31,80] and computer simulations[20] on polyelectrolytes show that salt can induce structural transitions in a polyelectrolyte. In the limit [salt] = 0, a strong polyelectrolyte adopts a rod-like structure[81] and it can undergo a transition from rod-like to SAW in the limit of infinite [salt].[29] We characterized prothymosin-α and sic1 behavior at different length scales as the [salt] is varied by extracting the scaling exponent ν from $S(q)$ (Figure 3C,D). In low [salt] (=0.01 M), prothymosin-α, which is a strong polyelectrolyte, behaves as a rod ($S(q) \sim q^{-1}$) (Figure 3C), whereas sic1, which is a weak polyelectrolyte, behaves as a SAW ($S(q) \sim q^{-5/3}$) (Figure 3D). With the increase in [salt], prothymosin-α switches from a rod-like behavior to SAW due to charge screening (Figure 3C). In a high concentration of KGlu ([KGlu] = 8 M), which stabilizes compact IDP conformations, prothymosin-α approaches ideal polymer chain behavior ($S(q) \sim q^{-2}$) (Figure 3C), whereas sic1 is on the verge of collapse to a globule because the value of ν is between the ideal chain and collapsed globule values ($1/3 < \nu < 1/2$) probably due to the finite length of sic1 (Figure 3D). At short length scales ($q > 3$ nm^{-1}), both prothymosin-α and sic1 behave as SAWs for all [salt] except for [KGlu] = 8 M, where they exhibit ideal chain behavior (Figure 3B,D).

We can rationalize our polyelectrolyte-like IDP results in strongly protective salt solutions using the self-consistent variational theory for the size of a polyelectrolyte chain in a poor solvent.[29] According to this theory, the effective excluded volume, which determines the size of the polymer, depends on two terms: (1) effective two-body interaction term in the absence of charges, which is negative in poor solvents, and (2) the second term, due to the charges present in the polymer, which is positive and increases with the net charge on the polymer. If both terms balance out, then the effective excluded volume is zero and the polymer behaves like an ideal chain. However, if the second term is larger due to a higher net charge per residue in the IDP, the effective excluded volume will be more positive and the polymer will be swollen.

Salt-Induced Transitions in Polyampholyte-like IDPs. A significant fraction of the IDPs are polyampholytes in nature.[82] Based on FCR, ERMTADn and IN are classified as strong polyampholytes (FCR $\geq$ 0.3). The $\langle R_g \rangle$ of ERMTADn increased from 31.75 to 36.0 Å with the increase in [salt] from 0 to 1 M (Figure 4A). In contrast to ERMTADn, the $\langle R_g \rangle$ of

https://doi.org/10.1021/acs.jpcb.2c03476
J. Phys. Chem. B 2022, 126, 5959−5971

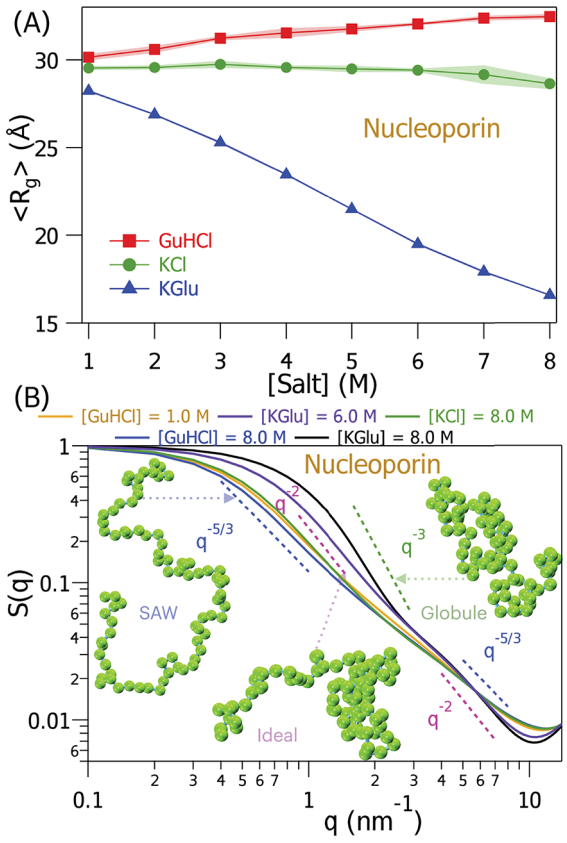

Figure 5. (A) $\langle R_g \rangle$ of nucleoporin as a function of [GuHCl] (red squares), [KCl] (green circles), and [KGlu] (blue triangles). (B) $S(q)$ of nucleoporin in the presence of [GuHCl] = 1 M (yellow) and 8 M (blue); [KCl] = 8 M (green); and [KGlu] = 6 M (violet) and 8 M (black). The dashed straight lines represent the globule (green), ideal chain (magenta), and SAW (blue) polymer chain configurations.

IN marginally decreased from 21.75 to 21.5 Å as the [salt] is increased to 0.15 M (Figure 4B). The opposite trend in $\langle R_g \rangle$ variation as a function of [salt] can be attributed to $\sigma_{\pm}$ and $SCD_{low\ salt}$ in ERMTADn ($\sigma_{\pm} \approx 0.007$, $SCD_{low\ salt} = -7.4$) and IN ($\sigma_{\pm} \approx 0.017$, $SCD_{low\ salt} = 10$) (Table S1). Expansion of ERMTADn ($SCD_{low\ salt} < 0$) and compaction of IN ($SCD_{low\ salt} > 0$) with the addition of salt in low [salt] are in compliance with the polyampholyte theory.[22,33,83]

ERMTADn, being a strong polyampholyte with low $\sigma_{\pm}$, behaves as an ideal chain in low [salt] (=0.01 M), and as the [salt] is increased, it approaches the SAW behavior (Figure 4C). IN is a polyampholyte with a large $\sigma_{\pm}$ in low [salt] (=0.01 M), and it behaves as a SAW for all concentrations of GuHCl and KCl (Figure 4D). Although ERMTADn and IN are strong polyampholytes, the type of conformations sampled by IDPs may differ in low [salt] due to differences in SCD[24] and the charge patterning parameter (κ).[21] ERMTADn (SCD = −1.06) is more compact than IN (SCD = 1.28) at [salt] = 0.01 M due to segregation of charges. The ideal chain behavior of ERMTADn ($\kappa = 0.22$) and SAW behavior of IN ($\kappa = 0.1$) at [salt] = 0.01 M is in accordance with the Flory random coil and excluded volume[21] limit of random polyampholytes, respectively, based on κ.

In high concentration of the strong protective salt KGlu ([KGlu] = 8.0 M), ERMTADn undergoes compaction and it is on the verge of collapse to a globule as $1/3 < \nu < 1/2$ (Figure 4C), and IN approaches ideal chain behavior (Figure 4D). Both ERMTADn and IN, at short length scales ($q > 3\ nm^{-1}$), behave as SAW for all [GuHCl] and [KCl], and in low [KGlu]. For [KGlu] = 8.0 M, even at smaller length scales, both ERMTADn and IN exhibit ideal chain behavior.

Salt-Induced Transitions in Uncharged IDP. We investigated the effect of salts on the structure of nucleoporin, which has no charged residues. Being devoid of charged residues, modulation of Coulombic interactions by salt does not apply to this IDP. The conformational ensemble of nucleoporin is affected by salt-specific Hofmeister effects. The salt-specific interactions with nucleoporin are similar to the other polypeptide chains investigated here. With the increase in [GuHCl] from 1 to 8 M, the $\langle R_g \rangle$ marginally increased from ≈30.14 to ≈32.5 Å. In the presence of protective osmolytes, KCl and KGlu, the $\langle R_g \rangle$ decreased with an increase in [salt]. However, the decrease in $\langle R_g \rangle$ is significantly different as KCl is a weakly stabilizing agent whereas KGlu is a strongly stabilizing agent. As [KCl] changed from 1 to 8 M, $\langle R_g \rangle$ of nucleoporin decreased by ≈0.9 Å, whereas, with the increase in [KGlu] from 1 to 8 M, the $\langle R_g \rangle$ decreased by ≈12.0 Å. Nucleoporin behaves like a SAW ($\nu \approx 3/5$) at all length scales for all concentrations of GuHCl and KCl and low concentration of KGlu ([KGlu] < 6 M) as inferred from $S(q)$. However, at higher concentration of KGlu ([KGlu] = 8 M) nucleoporin collapsed to a compact globule-like conformations ($\nu = 1/3$). At smaller length scale ($q > 4\ nm^{-1}$), the chain exhibits ideal polymer chain behavior.

IDP Conformations in High Concentration of Strongly Protective Salt. Depending on the polymer class to which the IDP belonged, it exhibited three kinds of behavior ($\nu = 1/2$, 2/5, and 1/3) in high concentrations of a strongly protective salt ([KGlu] = 8 M). The free energies for transferring the amino acid residues from water to a KGlu solution (δg_{tr}) are positive for all of the residues except for Asp and Asn.[55] Residue Phe has the maximum positive δg_{tr} value. As a result, in the KGlu solution, IDPs prefer to adopt compact conformations if they are devoid of Asp and Asn and coil-like conformations if they are rich in Asp and Asn.

In prothymosin-α, there are 19 (≈17%) Asp, 6 (≈5.45%) Asn, and 0 Phe residues. In IN there are 5 (≈8.9%) Asp, 2 (≈3.57%) Asn, and 2 (≈3.57%) Phe residues. Since both prothymosin-α and IN are rich in Asp and Asn, even when [KGlu] = 8 M, they exhibit ideal chain ($\nu = 1/2$) behavior (Figures 3C and 4D). The IDP nucleoporin contains only 3 (≈3.7%) Asn residues, which destabilize compact conformations. All of the other residues present in nucleoporin prefer compact conformations, and in addition it has 7 (≈8.4%) Phe residues, which strongly prefer compact conformations. As a result, when [KGlu] = 8 M, nucleoporin adopts a globular conformations ($\nu = 1/3$) (Figure 5B).

In sic1 and ERMTADn, the Asn and Asp residues are more in number than the Phe residues. In sic1, there are 6 (≈6.67%) Asn and 3 (≈3.33%) Phe residues, whereas in ERMTADn, there are 11 (≈9.02%) Asn, 3 (≈2.45%) Asp, and 6 (≈4.92%) Phe residues. When [KGlu] = 8 M, both sic1 and ERMTADn adopt neither the globule ensemble ($\nu = 1/3$) nor the ideal chain ensemble ($\nu = 1/2$). The value of ν obtained for both these IDPs is ≈2/5, which is between 1/3 and 1/2 (Figures 3D and 4C). To check if these IDPs at [KGlu] = 8 M are on the verge of collapse to a globule, we performed simulations in higher concentration, [KGlu] = 10 M, although a salt solution with this concentration is unphysical. We find that both of these IDPs collapse to a globule, yielding $\nu \approx 1/3$ (Figure S5),

https://doi.org/10.1021/acs.jpcb.2c03476
J. Phys. Chem. B 2022, 126, 5959−5971

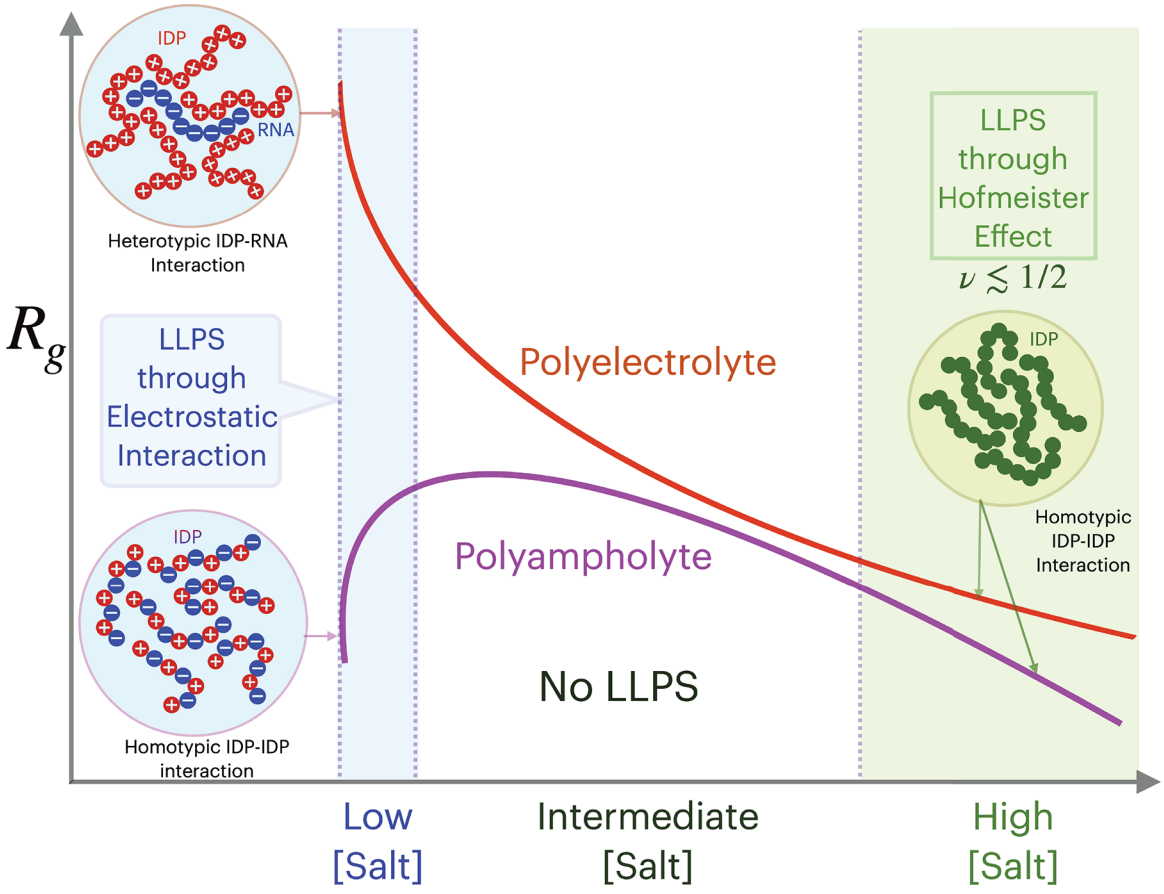

Figure 6. Prediction of IDP condensate formation from single-molecule salt-dependent properties. IDPs can form condensates in low and high [salt]. In low [salt], polyelectrolyte-like IDPs exhibit LLPS in the presence of oppositely charged ligands, whereas polyampholyte-like IDPs can undergo self-assembly without any ligands as they have both positively and negatively charged residues. In high [salt], the change in solvent quality due to the addition of salt leads to condensate formation by the IDPs. The quality of the solvent to the IDP modified by the addition of salt should be poorer than the ideal solvent conditions, $\nu \leq 1/2$.

confirming that both sic1 and ERMTADn, at [KGlu] = 8 M, with $\nu \approx 2/5$ are on the verge of collapse to a globule.

When [KGlu] = 6 M, sic1 and ERMTADn exhibit ideal chain behavior ($\nu \approx 1/2$). At [KGlu] = 8 M, where the IDPs yield $\nu \approx 2/5$, we computed the probability distribution of R_g, $P(R_g)$ to get an estimate into the population of IDPs conformations spanning between ideal chain conformations and globule conformations and compared it to those obtained at [KGlu] = 6 and 10 M (Figure S6). Computed $P(R_g)$ shows that, at [KGlu] = 8 M, there is a significant IDP population in both the globule and ideal chain conformations, which can result in a ν value of ≈2/5.

Role of Salt in the Formation of Biomolecular Condensates. Experiments[84−87] show that salts alter the propensities of IDPs/IDRs to exhibit LLPS by modulating electrostatic and hydrophobic interactions (Figure 6). Polymer theory based on random-phase-approximation[88] and computer simulations[36,42,89] demonstrated that the propensity of an IDP to exhibit LLPS is encoded in its single-molecular properties. These studies show that compaction of the IDP dimensions at the single-molecular level is correlated to exhibiting LLPS. The solvent conditions ($\nu \leq 1/2$) for which the IDP dimensions are smaller than the ideal chain are conducive to observing LLPS. Hence, sequence properties such as net charge/charge patterning[89] must play a key role in governing the LLPS propensity. The mechanism of condensate formation varies depending on [salt]. In low [salt], the LLPS propensity is controlled by electrostatic interactions independent of solvent quality, whereas, in high [salt], at least ideal solvent conditions are essential for phase separation.

In this work, we show that, in the low and high [salt] regimes, electrostatic interactions and Hofmeister effects govern the IDP single-chain behavior, respectively. We can now predict the solvent quality of a specific salt solution to an IDP by computing the exponent ν from simulations performed using the IDP coarse-grained model in conditions mimicking the salt concentration. Combining this capability with the result[36,88,89] that a correlation exists between the solvent quality to an IDP and IDPs propensity to exhibit LLPS, we can now predict whether an IDP in the semi-dilute regime can show LLPS when we vary the concentration of a specific salt.

In the low [salt] regime ([salt] $\lesssim$ 200 mM), polyelectrolyte-like IDPs such as prothymosin-α and sic1 are highly expanded due to electrostatic repulsion. Therefore, oppositely charged molecules such as RNA,[90−92] DNA, polylysine, or polyarginin are required to induce LLPS through a network of heterotypic interactions between the IDPs and ligands.[93,94] Conversely, polyampholyte-like IDPs such as ERMTADn and IN are stabilized due to attractive intramolecular electrostatic interactions between positively and negatively charged residues. Polyampholytes exhibit LLPS by forming a network of homotypic interactions[94] through self-association, and

https://doi.org/10.1021/acs.jpcb.2c03476
J. Phys. Chem. B 2022, 126, 5959−5971

ligands are not required. The IDP concentration must be in the semi-dilute regime to show phase separation. The critical IDP concentration required to exhibit phase separation for charged IDPs decreases with the increase in FCR and increases with [salt] in low [salt] regime.[92] Moreover, droplet stability of charged IDPs increases with FCR for a fixed [salt]. Additionally, the distribution of charged residues in the sequence must be considered to decipher the polymer−salt phase diagram, especially the nature of the tie line in the low [salt] regime.[95−97] Theories developed for uniformly distributed homopolyelectrolytes predict a tie line with a negative slope in the polymer−salt phase diagram.[95,96] In contrast, the theory to account for the non-uniform distribution of charged residues in the IDP sequences predicts a tie line with a positive slope.[97]

In the intermediate salt concentration regime (200 mM $\lesssim$ [salt] $\lesssim$ 2 M),[84,85] the electrostatic interactions are screened out and LLPS is not observed for both polyelectrolytes- and polyampholyte-like IDPs (Figure 6). Uncharged IDPs such as nucleoporin will not exhibit LLPS in low and intermediate [salt] due to the absence of charged residues and high solubility due to the polar residues present in the IDP.

IDPs can re-enter the demixed phase separated state from a well-mixed state exhibiting LLPS in high concentration of stabilizing salts,[84,85] through salt mediated Hofmeister effects[98] (Figure 6). Both charged and uncharged IDPs can form droplets if intramolecular monomer−monomer interaction is more favorable compared to monomer−solvent interaction at the single-molecular level ($\nu \lesssim 1/2$).[36,88,89] On the basis of the single-chain properties of polyelectrolyte IDPs (prothymosin and IN, (Figure 3C,D)), polyampholyte IDPs (ERMTADn and sic1 (Figure 4C,D)) and uncharged IDP (nucleoporin (Figure 5B)), we predict that these IDPs in the semi-dilute regime can re-enter the phase separated state in salt solutions, [KGlu] $\approx$ 8 M, as $\nu \lesssim 1/2$ for these IDPs.

CONCLUSIONS

We proposed a simulation methodology to study the effect of salts on IDPs using a reliable coarse-grained simulation model for the IDPs[35] and experimentally measured transfer free energy of amino acids from water to the salt solutions.[34,53] The method bridges a critical gap to understand the IDP properties in salt solutions, as salts are widely used to perturb IDP conformations to probe their role in biophysical phenomena or for use as biomaterials. Furthermore, the method overcomes the time scale problem associated with the all-atom simulations and the lack of reliable force fields to simulate high salt concentration solutions. The salt-induced transitions observed in the IDPs conformational ensemble with the variation in salt concentration depend on the polymer class of the IDP and salt identity. The role of charge composition and sequence in influencing the IDP structures in low ionic strength solutions where charge screening plays a dominant role is in accordance with the previous studies.[16,21,22] However, in high ionic strength solutions, the transitions observed in the conformational ensembles of IDPs depend on the salt identity. Using this simulation methodology, we studied the effect of multiple salts on the single-molecule properties of IDPs, which can predict whether the salt can induce LLPS in semi-dilute solutions of IDPs. The model makes it feasible to directly simulate the LLPS by various IDPs in different salt solutions to understand the mechanism and dynamics of IDP condensate formation.

ASSOCIATED CONTENT

Supporting Information

The Supporting Information is available free of charge at https://pubs.acs.org/doi/10.1021/acs.jpcb.2c03476.

Simulation methods and data analysis; (Table S1) primary sequences and classes; (Table S2) model parameters used; (Table S3) bead radii; (Figure S1) normalized scattering intensity profiles; (Figures S2 and S6) probabilities of nonlocal contact formation and of R_g; (Figure S3) interchain residue distance deviations; (Figure S4) dissecting electrostatic and Hofmeister effects; (Figure S5) structure factors; (Figure S7) end-to-end distance autocorrelation function (PDF)

AUTHOR INFORMATION

Corresponding Author

Govardhan Reddy − *Solid State and Structural Chemistry Unit, Indian Institute of Science, Bengaluru, Karnataka, India 560012;* orcid.org/0000-0002-9013-8040; Phone: +91-80-22933533; Email: greddy@iisc.ac.in; Fax: +91-80-23601310

Authors

Hiranmay Maity − *Solid State and Structural Chemistry Unit, Indian Institute of Science, Bengaluru, Karnataka, India 560012;* Present Address: (H.M.) Department of Chemistry, University of Texas at Austin, Austin, TX 78712, USA

Lipika Baidya − *Solid State and Structural Chemistry Unit, Indian Institute of Science, Bengaluru, Karnataka, India 560012*

Complete contact information is available at: https://pubs.acs.org/10.1021/acs.jpcb.2c03476

Author Contributions

‡H.M. and L.B. contributed equally to this work.

Notes

The authors declare no competing financial interest.

ACKNOWLEDGMENTS

G.R. acknowledges funding from Science and Engineering Research Board (EMR/2016/001356) and the National Supercomputing Mission (MeitY/R&D/HPC/2(1)/2014). H.M. acknowledges a research fellowship from Indian Institute of Science—Bangalore. L.B. acknowledges a research fellowship from the prime minister's research fellows (PMRFs) scheme. We acknowledge National Supercomputing Mission (NSM) for providing computing resources of "PARAM Brahma" at IISER Pune, which is implemented by C−DAC and supported by the Ministry of Electronics and Information Technology (MeitY) and Department of Science and Technology (DST), Government of India.

REFERENCES

(1) Dyson, H.; Wright, P. Intrinsically unstructured proteins and their functions. *Nat. Rev. Mol. Cell Biol.* **2005**, *6*, 197−208.

(2) Bondos, S. E.; Dunker, A. K.; Uversky, V. N. On the roles of intrinsically disordered proteins and regions in cell communication and signaling. *Cell Commun. Signal.* **2021**, *19*, 88.

(3) Riback, J. A.; Katanski, C. D.; Kear-Scott, J. L.; Pilipenko, E. V.; Rojek, A. E.; Sosnick, T. R.; Drummond, D. A. Stress-triggered phase

separation is an adaptive, evolutionarily tuned response. *Cell* **2017**, *168*, 1028−1040.
(4) Molliex, A.; Temirov, J.; Lee, J.; Coughlin, M.; Kanagaraj, A. P.; Kim, H. J.; Mittag, T.; Taylor, J. P. Phase separation by low complexity domains promotes stress granule assembly and drives pathological fibrillization. *Cell* **2015**, *163*, 123−133.
(5) Strom, A. R.; Emelyanov, A. V.; Mir, M.; Fyodorov, D. V.; Darzacq, X.; Karpen, G. H. Phase separation drives heterochromatin domain formation. *Nature* **2017**, *547*, 241−245.
(6) Alberti, S.; Dormann, D. Liquid-liquid phase separation in disease. *Annu. Rev. Genet.* **2019**, *53*, 171−194.
(7) Nozawa, R.-S.; Yamamoto, T.; Takahashi, M.; Tachiwana, H.; Maruyama, R.; Hirota, T.; Saitoh, N. Nuclear microenvironment in cancer: control through liquid-liquid phase separation. *Cancer Sci.* **2020**, *111*, 3155−3163.
(8) Ryan, V. H.; Fawzi, N. L. Physiological, pathological, and targetable membraneless organelles in neurons. *Trends Neurosci.* **2019**, *42*, 693−708.
(9) Shin, Y.; Brangwynne, C. P. Liquid phase condensation in cell physiology and disease. *Science* **2017**, *357*, eaaf4382.
(10) Okur, H. I.; Hladilkova, J.; Rembert, K. B.; Cho, Y.; Heyda, J.; Dzubiella, J.; Cremer, P. S.; Jungwirth, P. Beyond the Hofmeister series: ion-specific effects on proteins and their biological functions. *J. Phys. Chem. B* **2017**, *121*, 1997.
(11) Record, M. T., Jr; Guinn, E.; Pegram, L.; Capp, M. Introductory lecture: interpreting and predicting Hofmeister salt ion and solute effects on biopolymer and model processes using the solute partitioning model. *Faraday Discuss.* **2013**, *160*, 9−44.
(12) Baldwin, R. How Hofmeister ion interactions affect protein stability. *Biophys. J.* **1996**, *71*, 2056−2063.
(13) Xie, W. J.; Gao, Y. Q. Ion cooperativity and the effect of salts on polypeptide structure a molecular dynamics study of BBA5 in salt solutions. *Faraday Discuss.* **2013**, *160*, 191−206.
(14) Gao, Y. Q. Simple theory for salt effects on the solubility of amide. *J. Phys. Chem. B* **2012**, *116*, 9934−9943.
(15) Uversky, V. N.; Dunker, A. K. Understanding protein non-folding. *Biochim. Biophys. Acta* **2010**, *1804*, 1231−1264.
(16) Müller-Späth, S.; Soranno, A.; Hirschfeld, V.; Hofmann, H.; Rüegger, S.; Reymond, L.; Nettels, D.; Schuler, B. Charge interactions can dominate the dimensions of intrinsically disordered proteins. *Proc. Natl. Acad. Sci. U.S.A.* **2010**, *107*, 14609−14614.
(17) Vancraenenbroeck, R.; Harel, Y. S.; Zheng, W.; Hofmann, H. Polymer effects modulate binding affinities in disordered proteins. *Proc. Natl. Acad. Sci. U.S.A.* **2019**, *116*, 19506−19512.
(18) Hofmann, H.; Soranno, A.; Borgia, A.; Gast, K.; Nettels, D.; Schuler, B. Polymer scaling laws of unfolded and intrinsically disordered proteins quantified with single-molecule spectroscopy. *Proc. Natl. Acad. Sci. U.S.A.* **2012**, *109*, 16155−16160.
(19) Wohl, S.; Jakubowski, M.; Zheng, W. Salt-dependent conformational changes of intrinsically disordered proteins. *J. Phys. Chem. Lett.* **2021**, *12*, 6684−6691.
(20) Mao, A. H.; Crick, S. L.; Vitalis, A.; Chicoine, C. L.; Pappu, R. V. Net charge per residue modulates conformational ensembles of intrinsically disordered proteins. *Proc. Natl. Acad. Sci. U.S.A.* **2010**, *107*, 8183−8188.
(21) Das, R. K.; Pappu, R. V. Conformations of intrinsically disordered proteins are influenced by linear sequence distributions of oppositely charged residues. *Proc. Natl. Acad. Sci. U.S.A.* **2013**, *110*, 13392−13397.
(22) Samanta, H. S.; Chakraborty, D.; Thirumalai, D. Charge fluctuation effects on the shape of flexible polyampholytes with applications to intrinsically disordered proteins. *J. Chem. Phys.* **2018**, *149*, 163323.
(23) Firman, T.; Ghosh, K. Sequence charge decoration dictates coil-globule transition in intrinsically disordered proteins. *J. Chem. Phys.* **2018**, *148*, 123305.
(24) Sawle, L.; Ghosh, K. A theoretical method to compute sequence dependent configurational properties in charged polymers and proteins. *J. Chem. Phy* **2015**, *143*, 085101.
(25) Bowman, M. A.; Riback, J. A.; Rodriguez, A.; Guo, H.; Li, J.; Sosnick, T. R.; Clark, P. L. Properties of protein unfolded states suggest broad selection for expanded conformational ensembles. *Proc. Natl. Acad. Sci. U. S. A* **2020**, *117*, 23356−23364.
(26) Higgs, P.; Joanny, J. Theory of polyampholyte solutions. *J. Chem. Phys.* **1991**, *94*, 1543−1554.
(27) Das, R. K.; Ruff, K. M.; Pappu, R. V. Relating sequence encoded information to form and function of intrinsically disordered proteins. *Curr. Opin. Struct. Biol.* **2015**, *32*, 102−112.
(28) Muthukumar, M. Adsorption of a polyelectrolyte chain to a charged surface. *J. Chem. Phys.* **1987**, *86*, 7230−7235.
(29) Ha, B.-Y.; Thirumalai, D. Conformations of a polyelectrolyte chain. *Phys. Rev. A* **1992**, *46*, R3012−R3015.
(30) Dobrynin, A. V.; Rubinstein, M. Theory of polyelectrolytes in solutions and at surfaces. *Prog. Polym. Sci.* **2005**, *30*, 1049−1118.
(31) Muthukumar, M. 50th anniversary perspective: a perspective on polyelectrolyte solutions. *Macromolecules* **2017**, *50*, 9528−9560.
(32) Dobrynin, A.; Colby, R.; Rubinstein, M. Polyampholytes. *J. Polym. Sci. B: Polym. Phys.* **2004**, *42*, 3513−3538.
(33) Huihui, J.; Firman, T.; Ghosh, K. Modulating charge patterning and ionic strength as a strategy to induce conformational changes in intrinsically disordered proteins. *J. Chem. Phys.* **2018**, *149*, 085101.
(34) Pegram, L. M.; Wendorff, T.; Erdmann, R.; Shkel, I.; Bellissimo, D.; Felitsky, D. J.; Record, M. T., Jr. Why Hofmeister effects of many salts favor protein folding but not DNA helix formation. *Proc. Natl. Acad. Sci. U.S.A.* **2010**, *107*, 7716−7721.
(35) Baul, U.; Chakraborty, D.; Mugnai, M. L.; Straub, J. E.; Thirumalai, D. Sequence effects on size, shape, and structural heterogeneity in intrinsically disordered proteins. *J. Phys. Chem. B* **2019**, *123*, 3462−3474.
(36) Dignon, G. L.; Zheng, W.; Best, R. B.; Kim, Y. C.; Mittal, J. Relation between single-molecule properties and phase behavior of intrinsically disordered proteins. *Proc. Natl. Acad. Sci. U.S.A.* **2018**, *115*, 9929−9934.
(37) Song, J.; Li, J.; Chan, H. S. Small-Angle X-ray scattering signatures of conformational heterogeneity and homogeneity of disordered protein ensembles. *J. Phys. Chem. B* **2021**, *125*, 6451−6478.
(38) Rembert, K. B.; Paterova, J.; Heyda, J.; Hilty, C.; Jungwirth, P.; Cremer, P. S. Molecular mechanisms of ion-specific effects on proteins. *J. Am. Chem. Soc.* **2012**, *134*, 10039−10046.
(39) Shea, J.-E.; Best, R. B.; Mittal, J. Physics-based computational and theoretical approaches to intrinsically disordered proteins. *Curr. Opin. Struct. Biol.* **2021**, *67*, 219−225.
(40) Wu, H.; Wolynes, P. G.; Papoian, G. A. AWSEM-IDP: a coarse-grained force field for intrinsically disordered proteins. *J. Phys. Chem. B* **2018**, *122*, 11115−11125.
(41) Latham, A. P.; Zhang, B. Maximum entropy optimized force field for intrinsically disordered proteins. *J. Chem. Theory Comput.* **2020**, *16*, 773−781.
(42) Tesei, G.; Schulze, T. K.; Crehuet, R.; Lindorff-Larsen, K. Accurate model of liquid-liquid phase behavior of intrinsically disordered proteins from optimization of single-chain properties. *Proc. Natl. Acad. Sci. U. S. A* **2021**, *118*, e2111696118.
(43) Choi, J.-M.; Pappu, R. V. Improvements to the ABSINTH force field for proteins based on experimentally derived amino acid specific backbone conformational statistics. *J. Chem. Theory Comput.* **2019**, *15*, 1367−1382.
(44) Li, L.; Casalini, T.; Arosio, P.; Salvalaglio, M. Modeling the structure and interactions of intrinsically disordered peptides with multiple replica, metadynamics-based sampling methods and force-field combinations. *J. Chem. Theory Comput.* **2022**, *18*, 1915−1928.
(45) Huang, J.; Rauscher, S.; Nawrocki, G.; Ran, T.; Feig, M.; de Groot, B. L.; Grubmueller, H.; MacKerell, A. D., Jr. CHARMM36m: an improved force field for folded and intrinsically disordered proteins. *Nat. Methods* **2017**, *14*, 71−73.
(46) Oliveira Junior, A. B.; Lin, X.; Kulkarni, P.; Onuchic, J. N.; Roy, S.; Leite, V. B. P. Exploring energy landscapes of intrinsically

https://doi.org/10.1021/acs.jpcb.2c03476
J. Phys. Chem. B 2022, 126, 5959−5971

disordered proteins: insights into functional mechanisms. *J. Chem. Theory Comput.* **2021**, *17*, 3178−3187.
(47) Wang, W. Recent advances in atomic molecular dynamics simulation of intrinsically disordered proteins. *Phys. Chem. Chem. Phys.* **2021**, *23*, 777−784.
(48) Chong, S.-H.; Chatterjee, P.; Ham, S. Computer simulations of intrinsically disordered proteins. *Annu. Rev. Phys. Chem.* **2017**, *68*, 117−134.
(49) Pietrek, L. M.; Stelzl, L. S.; Hummer, G. Hierarchical ensembles of intrinsically disordered proteins at atomic resolution in molecular dynamics simulations. *J. Chem. Theory Comput.* **2020**, *16*, 725−737.
(50) Rauscher, S.; Gapsys, V.; Gajda, M. J.; Zweckstetter, M.; de Groot, B. L.; Grubmueller, H. Structural ensembles of intrinsically disordered proteins depend strongly on force field: a comparison to experiment. *J. Chem. Theory Comput.* **2015**, *11*, 5513−5524.
(51) O'Brien, E. P.; Ziv, G.; Haran, G.; Brooks, B. R.; Thirumalai, D. Effects of denaturants and osmolytes on proteins are accurately predicted by the molecular transfer model. *Proc. Natl. Acad. Sci. U.S.A.* **2008**, *105*, 13403−13408.
(52) Liu, Z.; Reddy, G.; Thirumalai, D. Theory of the molecular transfer model for proteins with applications to the folding of the src-SH3 domain. *J. Phys. Chem. B* **2012**, *116*, 6707−6716.
(53) Cheng, X.; Guinn, E. J.; Buechel, E.; Wong, R.; Sengupta, R.; Shkel, I. A.; Record, M. T., Jr. Basis of protein stabilization by K-Glutamate: unfavorable interactions with carbon, oxygen groups. *Biophys. J.* **2016**, *111*, 1854−1865.
(54) Record, M.; Anderson, C. Interpretation of preferential interaction coefficients of nonelectrolytes and of electrolyte ions in terms of a 2-domain model. *Biophys. J.* **1995**, *68*, 786−794.
(55) Maity, H.; Muttathukattil, A. N.; Reddy, G. Salt effects on protein folding thermodynamics. *J. Phys. Chem. Lett.* **2018**, *9*, 5063−5070.
(56) Mercadante, D.; Milles, S.; Fuertes, G.; Svergun, D. I.; Lemke, E. A.; Gräter, F. Kirkwood-Buff approach rescues overcollapse of a disordered protein in canonical protein force fields. *J. Phys. Chem. B* **2015**, *119*, 7975−7984.
(57) Lens, Z.; Dewitte, F.; Monté, D.; Baert, J.-L.; Bompard, C.; Sénéchal, M.; Van Lint, C.; de Launoit, Y.; Villeret, V.; Verger, A. Solution structure of the N-terminal transactivation domain of ERM modified by SUMO-1. *Biochem. Biophys. Res. Commun.* **2010**, *399*, 104−110.
(58) Mittag, T.; Marsh, J.; Grishaev, A.; Orlicky, S.; Lin, H.; Sicheri, F.; Tyers, M.; Forman-Kay, J. D. Structure/function implications in a dynamic complex of the intrinsically disordered sic1 with the cdc4 subunit of an SCF ubiquitin ligase. *Structure* **2010**, *18*, 494−506.
(59) Uversky, V. N.; Gillespie, J. R.; Millett, I. S.; Khodyakova, A. V.; Vasiliev, A. M.; Chernovskaya, T. V.; Vasilenko, R. N.; Kozlovskaya, G. D.; Dolgikh, D. A.; Fink, A. L.; et al. Natively unfolded human prothymosin-α adopts partially folded collapsed conformation at acidic pH. *Biochemistry* **1999**, *38*, 15009−15016.
(60) Bianchi, G.; Longhi, S.; Grandori, R.; Brocca, S. Relevance of electrostatic charges in compactness, aggregation, and phase separation of intrinsically disordered proteins. *Int. J. Mol. Sci.* **2020**, *21*, 6208.
(61) Hyeon, C.; Dima, R. I.; Thirumalai, D. Pathways and kinetic barriers in mechanical unfolding and refolding of RNA and proteins. *Structure* **2006**, *14*, 1633−1645.
(62) Maity, H.; Reddy, G. Thermodynamics and kinetics of single-chain monellin folding with structural insights into specific collapse in the denatured state ensemble. *J. Mol. Bio.* **2018**, *430*, 465−478.
(63) Maity, H.; Reddy, G. Folding of protein L with implications for collapse in the denatured state ensemble. *J. Am. Chem. Soc.* **2016**, *138*, 2609−2616.
(64) Reddy, G.; Liu, Z.; Thirumalai, D. Denaturant-dependent folding of GFP. *Proc. Natl. Acad. Sci. U.S.A* **2012**, *109*, 17832−17838.
(65) Reddy, G.; Thirumalai, D. Collapse precedes folding in denaturant-dependent assembly of ubiquitin. *J. Phys. Chem. B* **2017**, *121*, 995−1009.
(66) Reddy, G.; Thirumalai, D. Dissecting ubiquitin folding using the self-organized polymer model. *J. Phys. Chem. B* **2015**, *119*, 11358−11370.
(67) Maity, H.; Reddy, G. Transient intermediates are populated in the folding pathways of single-domain two-state folding protein L. *J. Chem. Phys.* **2018**, *148*, 165101.
(68) Humphrey, A.; Dalke, W.; Schulten, K. VMD − Visual Molecular Dynamics. *J. Mol. Graph.* **1996**, *14*, 33−38.
(69) Betancourt, M.; Thirumalai, D. Dissecting ubiquitin folding using the self-organized polymer model. *Protein Sci.* **1999**, *8*, 361−369.
(70) Chakraborty, D.; Straub, J. E.; Thirumalai, D. Differences in the free energies between the excited states of Aβ40 and Aβ42 monomers encode their aggregation propensities. *Proc. Natl. Acad. Sci. U. S. A.* **2020**, *117*, 19926−19937.
(71) Wodak, S. J.; Janin, J. Analytical approximation to the accessible surface area of proteins. *Proc. Natl. Acad. Sci. U.S.A.* **1980**, *77*, 1736−1740.
(72) Tong, S. D.; Yang; Lu, L. Accurate optimization of amino acid form factors for computing small angle X-ray scattering intensity of atomistic protein structures. *J. Appl. Crystallogr.* **2016**, *49*, 1148−1161.
(73) Rubinstein, M.; Colby, R. *Polymer Physics*; Oxford University Press: Oxford, U.K., 2003.
(74) Fuertes, G.; Banterle, N.; Ruff, K. M.; Chowdhury, A.; Mercadante, D.; Koehler, C.; Kachala, M.; Estrada Girona, G.; Milles, S.; Mishra, A.; et al. Decoupling of size and shape fluctuations in heteropolymeric sequences reconciles discrepancies in SAXS vs. FRET measurements. *Proc. Natl. Acad. Sci. U.S. A.* **2017**, *114*, E6342−E6351.
(75) Song, J.; Gomes, G.-N.; Shi, T.; Gradinaru, C. C.; Chan, H. S. Conformational heterogeneity and FRET data interpretation for dimensions of unfolded proteins. *Biophys. J.* **2017**, *113*, 1012−1024.
(76) Song, J.; Gomes, G.-N.; Gradinaru, C. C.; Chan, H. S. An adequate account of excluded volume is necessary to infer compactness and asphericity of disordered proteins by Forster Resonance Energy Transfer. *J. Phys. Chem. B* **2015**, *119*, 15191−15202.
(77) Lyle, N.; Das, R. K.; Pappu, R. V. A quantitative measure for protein conformational heterogeneity. *J. Chem. Phys.* **2013**, *139*, 121907.
(78) Fisher, M. Shape of a self-avoiding walk or polymer chain. *J. Chem. Phys.* **1966**, *44*, 616−622.
(79) Macdonald, D.; Hunter, D.; Kelly, K.; Jan, N. Self-avoiding walks in 2 to 5 dimensions - exact enumerations and series study. *J. Phys. A-Math. Gen.* **1992**, *25*, 1429−1440.
(80) Muthukumar, M. Dynamics of polyelectrolyte solutions. *J. Chem. Phys.* **1997**, *107*, 2619−2635.
(81) Barrat, J.; Joanny, J. Theory of polyelectrolyte solutions. In *Polymeric Systems*; Advances in Chemical Physics, Vol. *94*; Wiley, 1996; pp 1−66. DOI: 10.1002/9780470141533.ch1.
(82) Vucetic, S.; Obradovic, Z.; Vacic, V.; Radivojac, P.; Peng, K.; Iakoucheva, L.; Cortese, M.; Lawson, J.; Brown, C.; Sikes, J.; et al. DisProt: a database of protein disorder. *Bioinformatics* **2005**, *21*, 137−140.
(83) Ghosh, K.; Huihui, J.; Phillips, M.; Haider, A. Rules of physical mathematics govern intrinsically disordered proteins. *Annu. Rev. Biophys* **2022**, *51*, 355−376.
(84) Krainer, G.; Welsh, T. J.; Joseph, J. A.; Espinosa, J. R.; Wittmann, S.; de Csillery, E.; Sridhar, A.; Toprakcioglu, Z.; Gudiskyte, G.; Czekalska, M. A.; et al. Reentrant liquid condensate phase of proteins is stabilized by hydrophobic and non-ionic interactions. *Nat. Commun.* **2021**, *12*, 1085.
(85) Fetahaj, Z.; Ostermeier, L.; Cinar, H.; Oliva, R.; Winter, R. Biomolecular condensates under extreme martian salt conditions. *J. Am. Chem. Soc.* **2021**, *143*, 5247−5259.
(86) Nott, T. J.; Petsalaki, E.; Farber, P.; Jervis, D.; Fussner, E.; Plochowietz, A.; Craggs, T. D.; Bazett-Jones, D. P.; Pawson, T.; Forman-Kay, J. D.; et al. Phase transition of a disordered nuage

protein generates environmentally responsive membraneless organelles. *Mol. Cell* **2015**, *57*, 936−947.
(87) Agarwal, A.; Rai, S. K.; Avni, A.; Mukhopadhyay, S. An intrinsically disordered pathological prion variant Y145Stop converts into self-seeding amyloids via liquid-liquid phase separation. *Proc. Natl. Acad. Sci. U. S. A.* **2021**, *118*, e2100968118.
(88) Lin, Y.-H.; Chan, H. S. Phase separation and single-chain compactness of charged disordered proteins are strongly correlated. *Biophys. J.* **2017**, *112*, 2043−2046.
(89) Schuster, B. S.; Dignon, G. L.; Tang, W. S.; Kelley, F. M.; Ranganath, A. K.; Jahnke, C. N.; Simpkins, A. G.; Regy, R. M.; Hammer, D. A.; Good, M. C.; et al. Identifying sequence perturbations to an intrinsically disordered protein that determine its phase-separation behavior. *Proc. Natl. Acad. Sci. U.S.A.* **2020**, *117*, 11421−11431.
(90) Rai, S. K.; Savastano, A.; Singh, P.; Mukhopadhyay, S.; Zweckstetter, M. Liquid-liquid phase separation of tau: from molecular biophysics to physiology and disease. *Protein Sci.* **2021**, *30*, 1294−1314.
(91) Dutagaci, B.; Nawrocki, G.; Goodluck, J.; Ashkarran, A. A.; Hoogstraten, C. G; Lapidus, L. J; Feig, M. Charge-driven condensation of RNA and proteins suggests broad role of phase separation cytoplasmic environments. *eLife* **2021**, *10*, e64004.
(92) Elbaum-Garfinkle, S.; Kim, Y.; Szczepaniak, K.; Chen, C. C.-H.; Eckmann, C. R.; Myong, S.; Brangwynne, C. P. The disordered P granule protein LAF-1 drives phase separation into droplets with tunable viscosity and dynamics. *Proc. Natl. Acad. Sci. U. S. A* **2015**, *112*, 7189−7194.
(93) Mathieu, C.; Pappu, R. V.; Taylor, J. P. Beyond aggregation: pathological phase transitions in neurodegenerative disease. *Science* **2020**, *370*, 56−60.
(94) Mitrea, D. M.; Cika, J. A.; Stanley, C. B.; Nourse, A.; Onuchic, P. L.; Banerjee, P. R.; Phillips, A. H.; Park, C.-G.; Deniz, A. A.; Kriwacki, R. W. Self-interaction of NPM1 modulates multiple mechanisms of liquid-liquid phase separation. *Nat. Commun.* **2018**, *9*, 842.
(95) Zhang, P.; Shen, K.; Alsaifi, N. M.; Wang, Z.-G. Salt partitioning in complex coacervation of symmetric polyelectrolytes. *Macromolecules* **2018**, *51*, 5586−5593.
(96) Adhikari, S.; Leaf, M. A.; Muthukumar, M. Polyelectrolyte complex coacervation by electrostatic dipolar interactions. *J. Chem. Phys.* **2018**, *149*, 163308.
(97) Lin, Y.-H.; Brady, J. P.; Chan, H. S.; Ghosh, K. An unified analytical theory of heteropolymers for sequence-specific phase behaviors of polyelectrolytes and polyampholytes. *J. Chem. Phys.* **2020**, *152*, 045102.
(98) Lin, Y.; Fichou, Y.; Longhini, A. P.; Llanes, L. C.; Yin, P.; Bazan, G. C.; Kosik, K. S.; Han, S. Liquid-liquid phase separation of tau driven by hydrophobic interaction facilitates fibrillization of tau. *J. Mol. Bio.* **2021**, *433*, 166731.

https://doi.org/10.1021/acs.jpcb.2c03476
J. Phys. Chem. B 2022, 126, 5959−5971